DOI:
10.1515/nanoph-2021-0278

Document Version
Peer reviewed version

Research Article

A. Yu. Bykov*, D. J. Roth*, G. Sartorello, J. U. Salmón-Gamboa, and A. V. Zayats

Dynamics of Hot Carriers in Plasmonic Heterostructures

https://doi.org/10.1515/sample-YYYY-XXXX
Received Month DD, YYYY; revised Month DD, YYYY; accepted Month DD, YYYY

Abstract: Understanding and optimising the mechanisms of generation and extraction of hot carriers in plasmonic heterostructures is important for applications in new types of photodetectors, photochemistry and photocatalysis, as well nonlinear optics. Here, we show using transient dynamic measurements that the relaxation of the excited hot-carriers in Au/Pt hetero-nanostructures is accelerated through the transfer pathway from Au, where they are generated, to Pt nanoparticles, which act as a hot-electron sink. The influence of the environment on the dynamics was also demonstrated. The time-resolved photoluminescence measurements confirm the modified hot-electron dynamics, revealing quenching of the photoluminescence signal from Au nanoparticles in the presence of Pt and an increased photoluminescence lifetime. These observations are signatures of the improved extraction efficiency of hot-carriers by the Au/Pt heterostructures. The results give insight into the time-dependent behaviour of excited compound nanoscale systems and provide a way of controlling the relaxation mechanisms involved, with important consequences for engineering nonlinear optical response and hot-carrier-assisted photochemistry.

Keywords: plasmonic nanoparticles, hot electrons, carrier dynamics

***Corresponding author: A. Yu. Bykov, D. J. Roth,** Department of Physics and London Centre for Nanotechnology, King's College London, Strand, London WC2R 2LS, United Kingdom, e-mail: anton.bykov@kcl.ac.uk / diane.roth@kcl.ac.uk. These authors contributed equally to this work.

G. Sartorello, J. U. Salmón-Gamboa, A. V. Zayats, Department of Physics and London Centre for Nanotechnology, King's College London, Strand, London WC2R 2LS, United Kingdom

G. Sartorello, Current address: School of Applied and Engineering Physics, Cornell University, Ithaca, NY 14853, USA

1 Introduction

Optical properties of plasmonic nanoparticles have been extensively studied from both fundamental and application points of view. Strong local electromagnetic field enhancement and hot-carrier generation, both derived from localized surface plasmons (LSPs), are extremely beneficial for a variety of applications, such as enhancement of nonlinear optical effects [1, 2], chemical and biological sensing [3, 4], and optoelectronics [5]. Dynamics of the optically excited carriers in homogeneous plasmonic nanoparticles are reasonably well understood and explained through the sequence of radiative and non-radiative processes, governed by electron-electron, electron-phonon and electron-defect (or surface) scattering [6–9]. The relative contributions of these processes depends on the material of the nanoparticle, its size and shape.

Recently, with the development of photochemical and photocatalytic applications of plasmonic nanostructures, the focus has shifted from the study of pure plasmonic gold, silver, aluminium or copper nanoparticles to composite structures incorporating active catalytic metals, such as platinum or palladium [10–19]. Through photocatalytic transformations stimulated by hot electrons, it was inferred that in such hetero-structured nanoparticles, the light absorption in a plasmonic nanoparticle due to the LSP excitation efficiently creates hot electrons, which are then transferred to a catalytic nanoparticle [10]. The role of the latter is to facilitate the adsorption of molecular species and the hot-electron transfer from metal to the adsorbed molecule [20]. Such composite nanostructures have been shown to greatly promote the efficiency of liquid phase heterogeneous photocatalytic reactions, including CO_2 reduction [18], oxygen reduction [17] and organic pollutants decomposition, as studied in one of our previous work [19]. While reaction rates are generally improved with these plasmonic-based approaches, they are highly dependent on the design of the systems and the efficiency of the hot-carriers extraction process.

The time-resolved studies of the complex inter-veined carrier dynamic processes in bimetallic nanoparticles, including hot-carrier relaxation, transfer and extraction, are important to understand the beneficial design rules for heterostructured plasmonic nanoparticle photocatalysts. In this work, we investigate the hot-carrier dynamics in chemically-derived Au/Pt composite nanoparticles supported on silica (SiO_2) spheres, using time-resolved optical pump-probe and time-resolved photoluminescence spectroscopy, accessing both early stages of the dynamics before hot-electron thermalisation takes place, as well as the re-

laxation of thermalised electron gas in plasmonic hetero-nanoparticles. These nanoparticles exhibit an increased photocatalytic performance in photodegradation experiments of organic dyes via the generation of reactive oxygen species in water-based solvents [20]. The mechanism involves the interaction of hot-electrons excited in Au and transferred to Pt with oxygen molecules adsorbed on the Pt surface. The time-resolved optical pump-probe measurements show the enhanced rate of the hot-electron transfer from Au to Pt with the increase of the Pt concentration, as well as the role of scavenger molecules dissolved in the solvent on the hot-carrier dynamics. Additionally, the time-resolved photoluminescence measurements reveal a quenching of the photoluminescence signal from the Au nanoparticles in the presence of Pt and an increase in the photoluminescence lifetime, linked to charge separation in these nanoparticles. These results confirm the influence of the composition and surroundings on the hot-electron relaxation processes in bimetallic photocatalytic nanoparticles, important for rational design of plasmonic photocatalysts and composites with designed nonlinear optical response.

2 Results and discussion

Nanoparticle fabrication and properties

The nanoparticles studied in this work were fabricated by decorating large silica particles (150 nm in diameter) with gold nanoparticles (approximately 12 nm in diameter) produced by liquid phase chemical synthesis. The fabrication procedure of the SiO_2-Au-Pt hetero-nanoparticles is described in detail in Refs. [19, 20]. Large SiO_2 spheres were used as an inert support for the Au nanoparticles, both preventing aggregation of the Au nanoparticles in solution and also maximising the surface area available for the further deposition of Pt seeds, compared to Au films. The concentration of the SiO_2 nanoparticles solutions is ~ 0.15 nM. The amount of Au per SiO_2 nanoparticle is estimated to be 1.19×10^{-17} M. The Au nanoparticles are then coated with Pt seed nanoparticles of about 1-2 nm in diameter, forming a structure depicted in Figure 1b. During this process, Pt seeds selectively deposit onto the Au nanoparticles, not attaching elsewhere, therefore, forming a direct contact between Au and Pt. The in-depth study of the morphology of the hetero-nanoparticles, including transmission electron microscope (TEM) images, energy-dispersive X-ray spectroscopy (EDS) measurements, and elemental maps of their composition can be found in our previous papers [19, 20].

Nanoparticles with a varying concentration of Pt per SiO_2 nanoparticle were fabricated: SiO_2-Au-Pt (3.60×10^{-19} M of Pt/SiO_2 particle), SiO_2-Au-Pt_+ (7.22×10^{-19} M of Pt/SiO_2 particle), SiO_2-Au-Pt_{++} (1.44×10^{-18} M of Pt/SiO_2 particle), SiO_2-Au-Pt_{+++} (2.16×10^{-18} M of Pt/SiO_2 particle). These nanoparticles, initially fabricated in water, were also suspended in glycerol with much lower oxygen solubility than water.

The geometry of the hetero-nanoparticles, combining both a plasmonic metal and a metal more active catalytically, provides the advantage of a strong light absorption by the Au nanoparticles, together with an efficient electron extraction from the Au to the Pt, where the adsorbates taking part in chemical transformations are located. The presence of the nm-sized clusters of catalytic metal directly in contact with Au, with sharp curvature, provides a rough interface between Au and the surrounding environment. The numerical simulations show that these material and geometric properties lead to an additional electromagnetic field enhancement near the Au-Pt nanoparticle junctions [20] and, therefore, a high density of hot-spots, where hot-carriers are generated more efficiently. The strong electric field in these areas leads to the highest density of excited hot electrons and mark the locations where the photochemical reaction rates are increased [20]. The small size of the Pt nanoparticles also ensures the electron momentum relaxation, facilitating the electron transfer across the metal surface due to electron scattering to overcome momentum conservation.

Compared to metal/semiconductor hetero-structures relying on the design of an optimal charge barrier preventing fast electron-hole recombination [21, 22], the bimetallic hetero-nanoparticles do not exhibit any interfacial Schottky barrier through which the hot carriers have to tunnel, resulting in the availability of more hot carriers for catalytic processes with molecules adsorbed on the Pt surface [19, 20]. Time-resolved experiments on plasmonic-metal/semiconductor hybrids revealed various mechanisms for charged transfer dynamics across the metal/semiconductor interface, including hot electron injection, resonance energy transfer, plasmon-exciton coupling [23–26]. The role of trap states at the metal/semiconductor interface [27] and the plasmon energy renormalization due to charge transfer from semiconductor to a metal particle have also been demonstrated [28]. The bimetallic hetero-nanoparticles investigated here, in comparison, represent a simpler experimental system, while also exhibiting high photocatalytic performances. In addition, compared to their pure plasmonic counterparts, properly designed bimetallic hetero-nanoparticles generally demonstrate enhanced photocatalytic activity in various chemical reactions [11, 13, 14, 17]. In particular, the SiO_2-Au-Pt_{+++} hetero-nanoparticles studied in this work have been shown to perform better in the degradation of methylene blue organic dye than SiO_2-Au

nanoparticles [20], as well as other metal/semiconductor composite structures and bimetallic photocatalysts [29–32]. This degradation reaction is facilitated by the presence of reactive oxygen species, such as hydroxyl radical ($\cdot OH$) and superoxide anion radical ($\cdot O_2{}^-$), which are generated by the interaction of hot carriers with the surrounding aqueous medium. Photocatalytic experiments using different solvents and electron/hole scavengers demonstrated the dominant role of superoxide anion species in the degradation reaction [20].

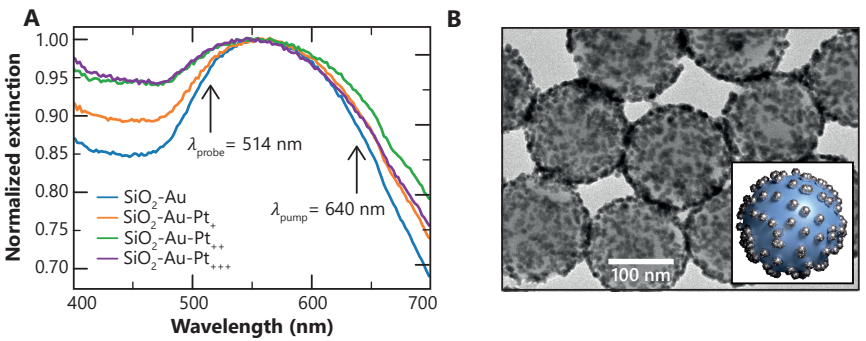

Fig. 1: (a) Normalized extinction spectra of the aqueous solution of SiO_2-Au and SiO_2-Au-Pt nanoparticles with varying concentration of Pt (see Nanoparticle fabrication section for the nanoparticle nomenclature). (b) TEM image of SiO_2-Au-Pt nanoparticles. Inset shows an artistic representation of the structure of a composite nanoparticle.

The extinction spectra of the SiO_2-Au nanoparticles suspended in water exhibit a LSP resonance in the 500–700 nm spectral range, with a maximum around 550 nm (Figure 1a). The broad nature of the extinction peak of the SiO_2-Au nanoparticles is mostly attributed to the increase of the Au particle size distribution during the growth of the Au nanoparticles onto the SiO_2 particles [20]. While pure Pt nanoparticles do not exhibit LSP in the visible spectral range, the addition of Pt to the SiO_2-Au nanoparticles leads to additional broadening of the LSP resonance, which can be related to the LSP dephasing arising from the presence of Pt nanoparticles in contact with Au nanoparticles. The width of the resonance increases with the concentration of Pt nanoparticles. This observed behaviour is in agreement with the numerical modelling of the optical response of the fabricated hetero-nanoparticles, which can be found in Refs. [19, 20].

Carrier dynamics for different catalytic metal loading

The two-colour time-resolved pump-probe measurements were performed in a collinear configuration with a 640-nm-wavelength pump and a 514-nm-wavelength probe. The pump wavelength was chosen to be in the vicinity of the LSP resonance (Figure 1a), while the choice of a probe wavelength allowed to clearly see the dynamics of the photoexcited hot-electron gas in Au, since photons at this wavelength have the energy close to the transition from the occupied d-band to the vicinity of the Fermi level [33]. As a probe, light from an Yb:KGW laser (Light Conversion Pharos, 230 fs pulses at 200 kHz) was used by converting the 1028 nm fundamental light to its second harmonic with a BBO crystal. The pump comes from a tuneable OPA (Light Conversion Orpheus) which is pumped by the same laser. The relative path length of pump and probe is adjusted by the use of a delay line, which is scanned from before to well after pulse coincidence for each measurement. The beams are made collinear by a mirror arrangement, and the probe is divided in a signal beam, passed through the sample, and a reference, which is routed around it. Pump and probe beams are focused inside a cuvette with the nanoparticle solution with a 25x reflective objective (Thorlabs LMM-25x-UVV). Signal and reference are aligned on the two photodiodes of a balanced detector. The detector is monitored with a lock-in amplifier (Stanford Research SR865A), which uses as its reference the frequency of an optical chopper positioned in the pump path.

Pump-probe traces for the nanoparticles with varying concentration of Pt in aqueous solution show the photo-induced transparency shortly after the interaction with the pump pulse (Figure 2a). This is consistent with the decreased absorption due to the conduction band states filling above the Fermi level in Au, that suppresses the optical transitions from the d-band to the conduction band at the probe wavelength. The transient absorption dependences were fitted with the combination of a single exponential decay, representing the cooling of the photoexcited hot-electron population, and a single exponential growth, representing the heating of the phonon bath. Such an assumption is valid in this case because the nanoparticles are smaller than the skin depth at the pump and probe wavelengths and, therefore, heating induced by the pump pulse can be considered uniform. We also do not take into consideration the initial nonequilibrium stage in the relaxation of the electron gas since it happens on the timescale shorter ($\sim$ 100 fs) than the (relatively long $\sim$ 150-200 fs) optical pulses used in this experiment [34]. The obtained two-exponential dependence is then convoluted with the Gaussian pulse cross-correlation function (Figure 2a).

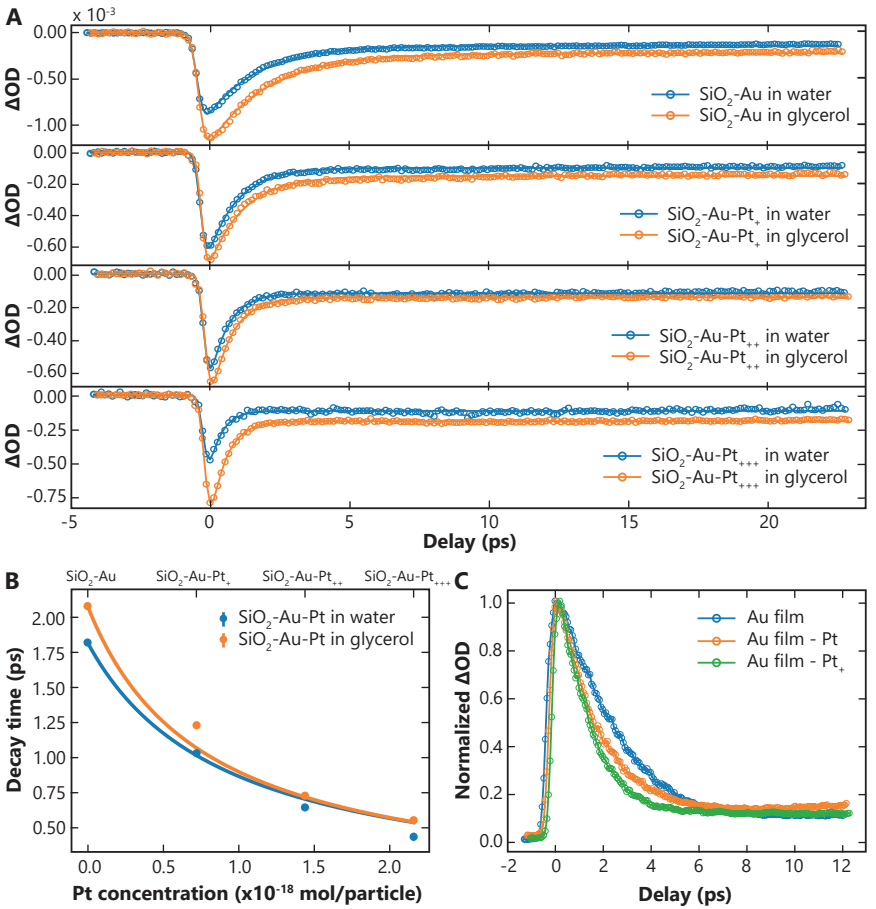

Fig. 2: (a) Pump-probe traces for SiO_2-Au-Pt with varying concentration of Pt in water and glycerol. **(b)** Dependence of the hot-electron decay time on the concentration of Pt for SiO_2-Au-Pt nanoparticles in (blue circles) water and (orange circles) glycerol. The lines correspond to an hyperbolic fit Eq. 2. **(c)** Normalized pump-probe traces for 15 nm Au films coated with Pt "seed" particles with two concentrations. See Nanoparticle fabrication section for details of nanoparticle concentrations in (a,b).

A prominent feature observed in the experiment is the substantial decrease in the temporal response of the nanoparticles with the increase of the Pt concentration. Due to much stronger electron-phonon coupling in Pt compared to Au, the hot electrons in bare Pt are expected to reach equilibrium with the lattice much faster than hot electrons in gold. However, when the metals are in

contact with each other, faster relaxation in Pt accelerates the energy relaxation in Au because of the increased hot-electron transfer across the interface in the attempt to achieve the thermodynamic equilibrium. Essentially, the Pt nanoparticles in contact with Au act as a sink for the hot-electron population, because electron-phonon coupling is much greater and the density of states at the Fermi level is higher in Pt. Similar behaviour has been observed before in Au/Pt core-shell particles [35] and multilayer gratings [36].

Microscopically, one can describe this behaviour by solving the nonlocal two-temperature model (TTM) with nonzero electron thermal conductivity [36]. However, for nanoscale metallic systems with length scales less than the free-electron mean-free path, the electron transfer happens much faster than the electron-phonon relaxation [37]. Therefore, without the loss of generality, one may obtain the final decay time, neglecting the non-thermalised electron extraction effects, by weighting the local responses of bulk gold and platinum with respect to their densities of states around the Fermi level as [35]

$$\frac{1}{\tau_{eff}}[N_{Pt}\rho\left(\epsilon_F\right)_{Pt} + N_{Au}\rho\left(\epsilon_F\right)_{Au}] = \frac{1}{\tau_{Pt}}N_{Pt}\rho\left(\epsilon_F\right)_{Pt} + \frac{1}{\tau_{Au}}N_{Au}\rho\left(\epsilon_F\right)_{Au} \quad (1)$$

where $N_{Pt/Au}$ is the number of atoms of Au and Pt in the bimetallic particle, respectively, and $\rho_{Pt/Au}$ is the density of states near the Fermi level of Pt and Au, respectively. It has been shown that for the complete Pt shells, the resulting relaxation time is mainly governed by the energy relaxation in Pt almost independently of the thickness of the shell [35]. However, in our case, the ability to control the Pt loading provides the means of tuning the temporal response of the composite structures. Following similar phenomenological reasoning that led to Eq. 1, we weight the decay time with respect to the total surface area of contact between Au and Pt through which the hot-electron transfer takes place. This surface area is assumed to be a linear function of the concentration. The corresponding fit

$$\tau_{eff}^{-1}(N) = \tau_{Au}^{-1}(1 + \alpha N) + \tau_{Pt}^{-1}\alpha N \quad (2)$$

is presented in Figure 2b, showing qualitative agreement with the experimental data.

In order to additionally confirm the role of the Pt contact to Au in the electron dynamics, we performed a series of pump-probe measurements using evaporated Au thin films in air coated with the similar Pt seed particles of two different concentrations (Au film - Pt and Au film - Pt_+, higher concentration).

Similar shortening of the decay time was indeed observed, albeit not so prominent due to much smaller contact surface area (Figure 2c).

Influence of the environment on carrier dynamics

Having established the mechanism of the photoexcited carrier dynamics in the particles, we now study a link between the hot electron dynamics and the photocatalytic response of the solutions. Identical solutions of SiO_2-Au and SiO_2-Au-Pt nanoparticles in water and glycerol were prepared. In contrast to water with significant concentration of dissolved oxygen, glycerol is known to have a much lower oxygen solubility [38]. The low concentration of oxygen in the glycerol solution limits the opportunity for hot-electron transfer from Pt to O_2 molecules adsorbed from water on a Pt surface, and has been shown to suppress the catalytic properties of the studied hetero-nanoparticles [20]. Here, we investigate how the oxygen solubility may influence the hot-electron dynamics in the hetero-nanoparticles. Optical transients obtained for nanoparticles in glycerol are plotted along the transients obtained for aqueous solutions (Figure 2a). The direct comparison shows a weaker amplitude of the pump-probe signals, as well as slightly reduced decay time in water, where additional hot-electron extraction channel exists (Figure 2b). The different electron-phonon thermalisation rates maybe related to the greater overall absorption of the pump radiation by nanoparticles in glycerol. This can be both due to stronger scattering of pump radiation in aqueous solution before the focus, where pump and probe beams overlap (due to higher refractive index contrast for water than glycerol) and higher absorption of nanoparticles in glycerol in the focus due to higher refractive index of surroundings. Therefore, under identical illumination condition, more energy of the pump beam is absorbed in the nanoparticles in glycerol leading to higher hot-electron temperatures. The hotter electron population then decays slower (Figure 2b) due to inherent nonlinearity of the two-temperature model (the decay time is proportional to $\gamma\Delta T_e/G$, where γ is the hot-electron heat capacity in a free-electron model, ΔT_e is the increase in the electron temperature and G is the phenomenological electron-phonon coupling constant). It is important to note that the observed change cannot be explained by the heat dissipation from the particles to the solvent, since the thermal conductivity of both solvents are small enough for this process to be much slower than the observed effect.

The carriers, which induce photodynamic transformations in adsorbates or surroundings, are likely to be nonthermalised carriers with high energies in the conduction band, produced by the light absorption. The lifetime of these hot

electrons far from the Fermi level, in addition to conventional thermalisation processes in metal, may also be determined by their transfer to the adjacent adsorbates before thermalisation. The modifications of the electron-phonon scattering dynamics in different solvents due to the electron transfer may not be sensitive enough on the background of the electron temperature variations discussed above, but the initial thermalisation rate is important. The initial thermalisation process, governed by the electron-electron scattering and the electron extraction, influences the initial rise time of the transient signal and its amplitude. The pulses used in this work have too long duration to resolve the rise-time variations (and the shorter pulses, such as those used for determining electron-electron scatting time in plasmonic CuS nanocrystals [39] are difficult to use with the solvent). The decreasing amplitude of the transient process with the increasing Pt loading (Figure 2a), for which the efficient hot-electron extraction increases and leads to the increased photocatalytic transformation [20], is observed in aqueous solution where oxygen is present but absent in glycerol solution. The amplitude is smallest for the nanoparticles for which hot-electron extraction is most effective.

Liquid phase photocatalytic system dynamics can be influenced by addition of electron or hole scavengers [20, 40, 41]. In this case, we can study the electron dynamics in the nanoparticles in the same aqueous solution to maintain the same absorbed energy, and monitor the influence of scavengers on the electron dynamics. Methanol (CH_3OH) was used as a hole scavenger (1.2 μL of 1M scavenger solution per 1 mL of nanoparticle solution) while $AgNO_3$ with the same concentration was used as an electron scavenger. This combination of scavengers have been used recently to assess the photocatalytic performance of the same nanoparticle system in the methylene blue (MB) photodegradation experiments [20]. It was demonstrated that the presence of methanol decreased the photodegradation of MB to a minor extent, while the addition of silver nitrate completely stopped the reaction, thus emphasizing the role of hot-electron pathway in the nanoparticle-driven visible light photocatalysis. The time-resolved optical measurements in an aqueous solution confirms the change of the carrier dynamics in the presence of scavengers (Figure 3).

While direct hot-electron transfer is not resolved in this experiment (as discussed above) as it is expected to happen on the femtosecond timescale and requires access to the initial non-equilibrium stage of the dynamics, we observe the aftermath of this process in the pump-probe traces. Indeed, the dissociated Ag^+ cations in water are acting as electron acceptors and are reduced into Ag^0, which is is deposited on the surface of the particles. This process then modifies the hot-carrier decay in the system in the same way as was observed above with

the addition of Pt. Since the electron-phonon coupling in Ag is much weaker than in Pt and in fact is close to the values of Au [42], this leads to the partial recovery of initial decay times of the pure Au nanoparticle composite (Figure 3a). The deposition of Ag on the nanoparticles is also observed in the linear optical properties of the hetero-nanoparticles (Figure 3b). At the same time, neither effect was observed when methanol was used as a hole scavenger since the hot-holes are weakly extracted and oxidation of methanol produces diluted chemical species that are not expected to interact with the hot carrier ensemble in the metallic system on picosecond timescales.

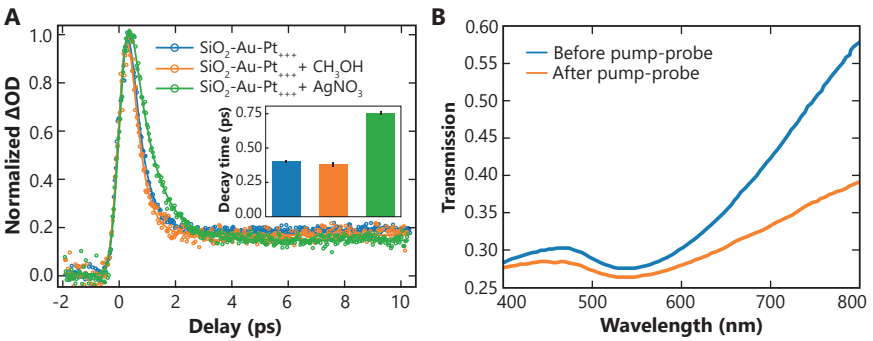

Fig. 3: (a) Pump-probe traces for SiO_2-Au-Pt_{+++} aqueous solution with electron ($AgNO_3$) or hole (CH_3OH) scavengers. **(b)** Optical transmission spectra of the SiO_2-Au-Pt_{+++} - $AgNO_3$ solution before and after pump-probe measurements.

Hot-carrier photoluminescence

The mechanism of photoluminescence from gold nanoparticles has for long been debated but it is now generally assigned to the recombination of photoexcited electrons with the d-band holes [43–45] and emission of the localised surface plasmons [46, 47]. This decay mechanism of the hot-electron population directly competes with thermalisation and nonradiative hot-electron transfer, but due to its low efficiency, its influence on the other relaxation channels is minimal, providing access to the non-equilibrium carrier distribution. It has been shown in various studies with bimetallic photocatalysts reporting photoluminescence measurements that the PL signal of plasmonic nanoparticles, such as gold, is quenched when a catalytic metal is added to the surface of the nanoparticles

[11–13]. This is a signature of the increase in the hot-carrier extraction efficiency from the plasmonic nanoparticle due to the presence of the catalytic metal. While time-resolved PL studies of bimetallic nanoparticles are quite sparse, time-resolved PL of plasmonic nanoparticles, such as gold, has been reasonably investigated. Results of these studies, however, performed with different types of experimental setups including time-correlated single photon counting, streak cameras and femtosecond up-conversion techniques, are relatively divergent and report very different decay times ranging from tens of femtoseconds to nanoseconds [46–50], depending also on the nanoparticle fabrication process. Some results also appear to be limited by the instrumental response of the systems used [46–48].

We used both PL spectroscopy and time-resolved PL based on a time-correlated single photon counting technique [38, 51] in order to get insight in the hot-carrier extraction process from the Au/Pt nanoparticles. The light emission from hot-carrier recombination can take place at different stages of the carrier relaxation, for which the corresponding dipolar transitions and local density of photonic states provide favorable conditions. Since the rate of the PL transitions is several orders of magnitude lower that electron-electron scattering rate, this decay channel has little influence on the other relaxation channels and can serve as a probe for the hot carrier properties.

Photoluminescence measurements from SiO_2-Au and SiO_2-Au-Pt_{+++} nanoparticles suspended in both water and glycerol were performed. The concentration of SiO_2 nanoparticles solutions in these PL experiments is $\sim$ 0.45 nM. Light from a supercontinuum laser (20 MHz repetition rate, 400 fs pulse, 1 mW average power, Fianium), filtered with a 10 nm bandpass filter centered at 488 nm (ZET488/10x, Chroma), was focused through a cuvette using a microscope objective (50x, NA = 0.5, Olympus) and the PL signal was collected via the same objective. A 20 nm bandpass filter centered on 642 nm (ZET642/20x, Chroma) and a 600 nm longpass (FELH600, Thorlabs) filter were used in order to record the PL emission decay dynamics of the nanoparticles. Photoluminescence spectra were recorded using a QE Pro 65000 spectrometer (Ocean Optics), with a 500 nm longpass filter (FELH500, Thorlabs) to remove any contribution from the laser to the photoluminescence signal.

The decay dynamics of the various nanoparticles (Figure 4(b,e)) were then analysed using an inverse Laplace transform method [51], allowing the determination of the lifetime distributions of the PL from SiO_2-Au and SiO_2-Au-Pt_{+++} nanoparticles in different environments. This method does not require any preliminary estimation of the lifetime distribution and is based on the solution of

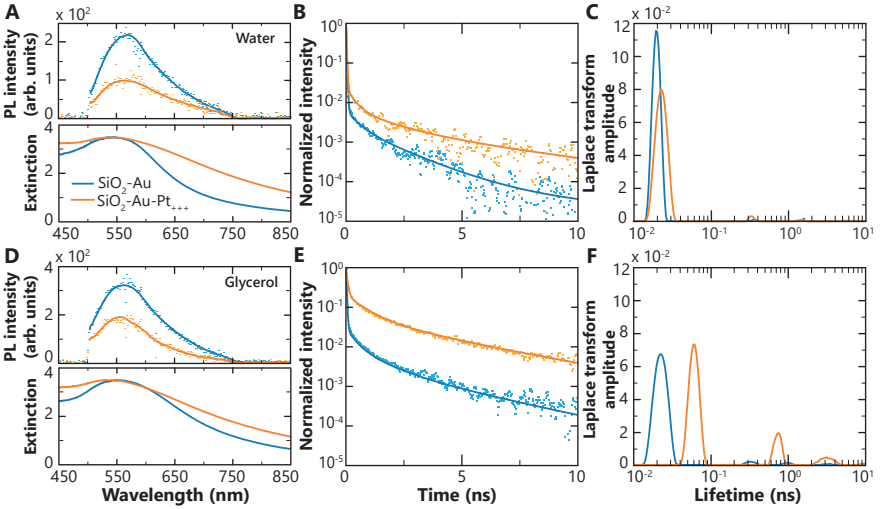

Fig. 4: (a,d) Photoluminescence (top) and extinction (bottom) spectra. (b,e) Normalised decay dynamics deconvoluted from the experimental instrumental response function of the system. (c,f) Laplace transform amplitude of SiO_2-Au (blue lines) and SiO_2-Au-Pt_{+++} (orange lines) nanoparticles in (a,b,c) water and (d,e,f) glycerol. The excitation wavelength is 488 nm.

the equation

$$I(t) = \int_0^\infty F(\tau) e^{\frac{-t}{\tau}} d\tau \tag{3}$$

where $I(t)$ is the measured decay deconvoluted from the experimental instrumental response function of the system and $F(\tau)$ is the relative weight of the exponential decay components. In order to account for the noise in the experimental PL decays and, therefore, the ill-defined character of inverse methods, an iterative fitting was performed to obtain stable results.

The PL spectra, extinction spectra and lifetime distributions for several combination of nanoparticle types and solvents are presented in Figure 4. The PL spectra show a peak centered around 550 nm, consistent with the gold luminescence peak arising from the electron-hole recombination near the L-symmetry point in the Brillouin zone [43, 44]. At the same time the position and shape of the PL spectra follow the position and shape of the extinction spectra (Figure 4a,d), being determined by the local density of state profile associated with the LSPs. The decay times observed in these experiments are in

the tens of picoseconds range, consistent with those reported in Refs. [49, 52]. Following the literature, we attribute the difference between the relaxation timescales observed in the pump-probe and PL studies to the recombination of electrons near the Fermi level. Faster, picosecond decay processes are not resolved in the PL experiments due to the instrumental response function. While the extinction of the nanoparticles in glycerol and water are similar, the PL intensity is higher in glycerol, where there is no hot-electron extraction channel to dissolved oxygen molecules; the difference is especially pronounced for Pt-containing hetero-nanoparticles with the PL intensity about 50% lower in water (Figure 4a,d). The influence of the solvent is also evident from the extracted lifetime components (Figure 4c,f). The dominant component of the PL lifetime of the pure Au nanoparticles practically does not depend on the solvent. At the same time, for the Au-Pt hetero-nanoparticles, the dominant PL time is longer than for the pure Au nanoparticles in glycerol, but almost the same in water. This confirms the role of the additional hot-electron extraction channels in the electron dynamics of the hetero-nanoparticles.

It should be noted that the energy distributions of hot-carriers generated through LSPs and by direct light absorption can be significantly different. Additionally, non-instantaneous excitation pulse, compared to the carrier relaxation time, may lead to the electron-hole pair accumulation during the excitation, influencing the PL dynamics. For pump-probe measurements, the LSP-enhanced free-carrier absorption only generates the hot-carrier distribution around the Fermi level in the conduction band. In the PL measurements, the shorter-wavelength excitation photon (488 nm) may be absorbed through both the interband transitions in Au and the LSP excitation. The excited hot carriers may be either extracted from Au (and a hetero-nanoparticle) or thermalise through multiple scattering (effectively increasing the electron population at lower energy states). In the absence of the hot-electron receptor in a glycerol solvent, the PL time is longer as the electron-hole pair is spatially separated after the electron transfer to Pt. However, when oxygen molecules are present in water, the hot-electron can be transferred to them leading to the drop in the PL intensity and removal of the long component from the PL lifetime.

3 Conclusion

The relaxation of excited hot-carriers in Au/Pt hetero-nanostructures was investigated using transient dynamic measurements and time-resolved photolumi-

nescence. Our results show that, on the picosecond timescales, the relaxation of the photoexcited hot-electron gas is accelerated in the presence of Pt, due to an increase in the hot-electron transfer across the gold-platinum interface and stronger electron-phonon interaction in platinum. Variable concentration of Pt in the hetero-nanoparticles allows controlling this process quantitatively. It was shown that the environment only weakly affects the hot-electron dynamics on the time scales of the electron-phonon interaction, however signatures of electron transfer to the surroundings can be observed in the amplitude of the pump-probe traces and the modifications of the electron-phonon coupling after photocatalytic decomposition observed in the experiment with hot-electron scavengers. The time-resolved photoluminescence measurements revealed that the presence of Pt lead to a decrease of the photoluminescence intensity of the Au nanoparticles, particularly prominent in an aqueous solution, where the pathway for the electron extraction to oxygen molecules from the non-equilibrium distribution is present.

This combination of pump-probe and time-resolved PL measurements shed light on the hot-carriers relaxation mechanisms of bimetallic hetero-nanostructures and the influence of the environment on the electron dynamics, which is of significant interest in the development of efficient hot-carrier-assisted photocatalysts as well as plasmon-semiconductor based devices.

Acknowledgments

This work was supported by EPSRC (UK) under the Reactive Plasmonics Programme grant (EP/M013812/1).

References

[1] M. Kauranen and A. V. Zayats, "Nonlinear plasmonics," *Nat. Photonics*, vol. 6, no. 11, pp. 737–748, 2012.

[2] A. E. Minovich, A. E. Miroshnichenko, A. Y. Bykov, T. V. Murzina, D. N. Neshev, and Y. S. Kivshar, "Functional and nonlinear optical metasurfaces," *Laser Photonics Rev.*, vol. 9, no. 2, pp. 195–213, 2015.

[3] D. Sil, K. D. Gilroy, A. Niaux, A. Boulesbaa, S. Neretina, and E. Borguet, "Seeing is believing: Hot electron based gold nanoplasmonic optical hydrogen sensor," *ACS Nano*, vol. 8, no. 8, pp. 7755–7762, 2014.

[4] C. Wang, X.-G. Nie, Y. Shi, Y. Zhou, J.-J. Xu, X.-H. Xia, and H.-Y. Chen, "Direct plasmon-accelerated electrochemical reaction on gold nanoparticles," *ACS Nano*, vol. 11, no. 6, pp. 5897–5905, 2017.

[5] K. Tielrooij, J. Song, S. A. Jensen, A. Centeno, A. Pesquera, A. Z. Elorza, M. Bonn, L. Levitov, and F. Koppens, "Photoexcitation cascade and multiple hot-carrier generation in graphene," *Nat. Phys.*, vol. 9, no. 4, pp. 248–252, 2013.

[6] S. Anisimov, B. Kapeliovich, and T. Perelman, "Electron emission from metal surfaces exposed to ultrashort laser pulses," *Zh. Eksp. Teor. Fiz*, vol. 66, pp. 375–377, 1974.

[7] P. B. Allen, "Theory of thermal relaxation of electrons in metals," *Phys. Rev. Lett.*, vol. 59, pp. 1460–1463, 1987.

[8] C.-K. Sun, F. Vallée, L. H. Acioli, E. P. Ippen, and J. G. Fujimoto, "Femtosecond-tunable measurement of electron thermalization in gold," *Phys. Rev. B*, vol. 50, pp. 15337–15348, Nov 1994.

[9] L. Nicholls, T. Stefaniuk, M. Nasir, F. Rodríguez-Fortuño, W. GA, and A. Zayats, "Designer photonic dynamics by using non-uniform electron temperature distribution for on-demand all-optical switching times," *Nat. Commun.*, vol. 10, no. 10, p. 2967, 2019.

[10] K. Sytwu, M. Vadai, and J. A. Dionne, "Bimetallic nanostructures: combining plasmonic and catalytic metals for photocatalysis," *Adv. Phys.: X*, vol. 4, no. 1, p. 1619480, 2019.

[11] Z. Zheng, T. Tachikawa, and T. Majima, "Single-particle study of pt-modified au nanorods for plasmon-enhanced hydrogen generation in visible to near-infrared region," *J. Am. Chem. Soc.*, vol. 136, no. 19, pp. 6870–6873, 2014.

[12] Z. Zheng, T. Tachikawa, and T. Majima, "Plasmon-enhanced formic acid dehydrogenation using anisotropic pd–au nanorods studied at the single-particle level," *J. Am. Chem. Soc.*, vol. 137, no. 2, pp. 948–957, 2015.

[13] Z. Lou, M. Fujitsuka, and T. Majima, "Pt–au triangular nanoprisms with strong dipole plasmon resonance for hydrogen generation studied by single-particle spectroscopy," *ACS Nano*, vol. 10, no. 6, pp. 6299–6305, 2016.

[14] U. Aslam, S. Chavez, and S. Linic, "Controlling energy flow in multimetallic nanostructures for plasmonic catalysis," *Nat. Nanotechnol.*, vol. 12, no. 10, pp. 1000–1005, 2017.

[15] S.-C. Lin, C.-S. Hsu, S.-Y. Chiu, T.-Y. Liao, and H. M. Chen, "Edgeless ag–pt bimetallic nanocages: in situ monitor plasmon-induced suppression of hydrogen peroxide formation," *J. Am. Chem. Soc.*, vol. 139, no. 6, pp. 2224–2233, 2017.

[16] S. Sarina, H. Zhu, E. Jaatinen, Q. Xiao, H. Liu, J. Jia, C. Chen, and J. Zhao, "Enhancing catalytic performance of palladium in gold and palladium alloy nanoparticles for organic synthesis reactions through visible light irradiation at ambient temperatures," *J. Am. Chem. Soc.*, vol. 135, no. 15, pp. 5793–5801, 2013.

[17] A. Holewinski, J.-C. Idrobo, and S. Linic, "High-performance ag–co alloy catalysts for electrochemical oxygen reduction," *Nat. Chem.*, vol. 6, no. 9, pp. 828–834, 2014.

[18] D. M. Hofmann, D. H. Fairbrother, R. J. Hamers, and C. J. Murphy, "Two-phase synthesis of gold–copper bimetallic nanoparticles of tunable composition: Toward optimized catalytic CO_2 reduction," *ACS Appl. Nano Mater.*, vol. 2, no. 6, pp. 3989–3998, 2019.

[19] J. U. Salmón-Gamboa, M. Romero-Gómez, D. J. Roth, M. J. Barber, P. Wang, S. M. Fairclough, M. E. Nasir, A. V. Krasavin, W. Dickson, and A. V. Zayats, "Optimizing hot carrier effects in pt-decorated plasmonic heterostructures," *Faraday Discuss.*, vol. 214, pp. 387–397, 2019.

[20] J. U. Salmón-Gamboa, M. Romero-Gómez, D. J. Roth, A. V. Krasavin, P. Wang, W. Dickson, and A. V. Zayats, "Rational design of bimetallic photocatalysts based on plasmonically-derived hot carriers," *Nanoscale Adv.*, vol. 3, no. 3, pp. 767–780, 2021.
[21] N. Wu, "Plasmonic metal–semiconductor photocatalysts and photoelectrochemical cells: a review," *Nanoscale*, vol. 10, no. 6, pp. 2679–2696, 2018.
[22] Y. Zhang, S. He, W. Guo, Y. Hu, J. Huang, J. R. Mulcahy, and W. D. Wei, "Surface-plasmon-driven hot electron photochemistry," *Chem. Rev.*, vol. 118, no. 6, pp. 2927–2954, 2017.
[23] K. Wu, J. Chen, J. R. McBride, and T. Lian, "Efficient hot-electron transfer by a plasmon-induced interfacial charge-transfer transition," *Science*, vol. 349, no. 6248, pp. 632–635, 2015.
[24] C. Clavero, "Plasmon-induced hot-electron generation at nanoparticle/metal-oxide interfaces for photovoltaic and photocatalytic devices," *Nat. Photonics*, vol. 8, no. 2, pp. 95–103, 2014.
[25] S. Tan, A. Argondizzo, J. Ren, L. Liu, J. Zhao, and H. Petek, "Plasmonic coupling at a metal/semiconductor interface," *Nat. Photonics*, vol. 11, no. 12, pp. 806–812, 2017.
[26] X.-C. Ma, Y. Dai, L. Yu, and B.-B. Huang, "Energy transfer in plasmonic photocatalytic composites," *Light: Sci. Appl.*, vol. 5, no. 2, pp. e16017–e16017, 2016.
[27] R. Jiang, B. Li, C. Fang, and J. Wang, "Metal/semiconductor hybrid nanostructures for plasmon-enhanced applications," *Adv. Mater.*, vol. 26, no. 31, pp. 5274–5309, 2014.
[28] D. Mongin, E. Shaviv, P. Maioli, A. Crut, U. Banin, N. Del Fatti, and F. Vallée, "Ultrafast photoinduced charge separation in metal–semiconductor nanohybrids," *ACS Nano*, vol. 6, no. 8, pp. 7034–7043, 2012.
[29] P. Prasannalakshmi and N. Shanmugam, "Fabrication of TiO_2/zno nanocomposites for solar energy driven photocatalysis," *Mater. Sci. Semicond. Process.*, vol. 61, pp. 114–124, 2017.
[30] M. Pirhashemi and A. Habibi-Yangjeh, "Ultrasonic-assisted preparation of plasmonic zno/ag/Ag_2WO_4 nanocomposites with high visible-light photocatalytic performance for degradation of organic pollutants," *J. Colloid Interface Sci.*, vol. 491, pp. 216–229, 2017.
[31] M. M. J. Sadiq, U. S. Shenoy, and D. K. Bhat, "$NiWO_4$-zno-nrgo ternary nanocomposite as an efficient photocatalyst for degradation of methylene blue and reduction of 4-nitro phenol," *J. Phys. Chem. Solids*, vol. 109, pp. 124–133, 2017.
[32] D. Kumar, S. B. Lee, C. H. Park, and C. S. Kim, "Impact of ultrasmall platinum nanoparticle coating on different morphologies of gold nanostructures for multiple one-pot photocatalytic environment protection reactions," *ACS Appl. Mater. Interfaces*, vol. 10, no. 1, pp. 389–399, 2018.
[33] R. W. Schoenlein, W. Z. Lin, J. G. Fujimoto, and G. L. Eesley, "Femtosecond studies of nonequilibrium electronic processes in metals," *Phys. Rev. Lett.*, vol. 58, pp. 1680–1683, Apr 1987.
[34] A. M. Brown, R. Sundararaman, P. Narang, A. M. Schwartzberg, W. A. Goddard, and H. A. Atwater, "Experimental and ab initio ultrafast carrier dynamics in plasmonic nanoparticles," *Phys. Rev. Lett.*, vol. 118, p. 087401, Feb 2017.
[35] J. H. Hodak, A. Henglein, and G. V. Hartland, "Tuning the spectral and temporal response in PtAu core–shell nanoparticles," *J. Chem. Phys.*, vol. 114, pp. 2760–2765, feb 2001.

[36] S. Edward, A. Antoncecchi, H. Zhang, H. Sielcken, S. Witte, and P. C. M. Planken, "Detection of periodic structures through opaque metal layers by optical measurements of ultrafast electron dynamics," *Opt. Express*, vol. 26, pp. 23380–23396, Sep 2018.

[37] G. Tagliabue, A. S. Jermyn, R. Sundararaman, A. J. Welch, J. S. DuChene, R. Pala, A. R. Davoyan, P. Narang, and H. A. Atwater, "Quantifying the role of surface plasmon excitation and hot carrier transport in plasmonic devices," *Nat. Commun.*, vol. 9, no. 1, pp. 1–8, 2018.

[38] D. J. Roth, P. Ginzburg, L. M. Hirvonen, J. A. Levitt, M. E. Nasir, K. Suhling, D. Richards, V. A. Podolskiy, and A. V. Zayats, "Singlet–triplet transition rate enhancement inside hyperbolic metamaterials," *Laser Photonics Rev.*, vol. 13, no. 9, p. 1900101, 2019.

[39] A. Y. Bykov, A. Shukla, M. van Schilfgaarde, M. A. Green, and A. V. Zayats, "Ultrafast carrier and lattice dynamics in plasmonic nanocrystalline copper sulfide films," *Laser Photonics Rev.*, p. 2000346, 2021.

[40] M. F. R. Samsudin, L. T. Siang, S. Sufian, R. Bashiri, N. M. Mohamed, and R. M. Ramli, "Exploring the role of electron-hole scavengers on optimizing the photocatalytic performance of $BiVO_4$," *Mater. Today: Proc.*, vol. 5, no. 10, pp. 21703–21709, 2018.

[41] M. Shen and M. A. Henderson, "Identification of the active species in photochemical hole scavenging reactions of methanol on TiO_2," *J. Phys. Chem. Lett.*, vol. 2, no. 21, pp. 2707–2710, 2011.

[42] Z. Lin, L. V. Zhigilei, and V. Celli, "Electron-phonon coupling and electron heat capacity of metals under conditions of strong electron-phonon nonequilibrium," *Phys. Rev. B*, vol. 77, p. 075133, Feb 2008.

[43] A. Mooradian, "Photoluminescence of metals," *Phys. Rev. Lett.*, vol. 22, pp. 185–187, Feb 1969.

[44] G. T. Boyd, Z. H. Yu, and Y. R. Shen, "Photoinduced luminescence from the noble metals and its enhancement on roughened surfaces," *Phys. Rev. B*, vol. 33, pp. 7923–7936, Jun 1986.

[45] J. Zheng, C. Zhou, M. Yu, and J. Liu, "Different sized luminescent gold nanoparticles," *Nanoscale*, vol. 4, no. 14, pp. 4073–4083, 2012.

[46] E. Dulkeith, T. Niedereichholz, T. Klar, J. Feldmann, G. Von Plessen, D. Gittins, K. Mayya, and F. Caruso, "Plasmon emission in photoexcited gold nanoparticles," *Phys. Rev. B*, vol. 70, no. 20, p. 205424, 2004.

[47] D. Huang, C. P. Byers, L.-Y. Wang, A. Hoggard, B. Hoener, S. Dominguez-Medina, S. Chen, W.-S. Chang, C. F. Landes, and S. Link, "Photoluminescence of a plasmonic molecule," *ACS Nano*, vol. 9, no. 7, pp. 7072–7079, 2015.

[48] E. Sakat, I. Bargigia, M. Celebrano, A. Cattoni, S. Collin, D. Brida, M. Finazzi, C. D'andrea, and P. Biagioni, "Time-resolved photoluminescence in gold nanoantennas," *ACS Photonics*, vol. 3, no. 8, pp. 1489–1493, 2016.

[49] K. Imura, T. Nagahara, and H. Okamoto, "Near-field two-photon-induced photoluminescence from single gold nanorods and imaging of plasmon modes," *J. Phys. Chem. B*, vol. 109, no. 27, pp. 13214–13220, 2005.

[50] Y.-N. Hwang, D. H. Jeong, H. J. Shin, D. Kim, S. C. Jeoung, S. H. Han, J.-S. Lee, and G. Cho, "Femtosecond emission studies on gold nanoparticles," *J. Phys. Chem. B*, vol. 106, no. 31, pp. 7581–7584, 2002.

[51] P. Ginzburg, D. J. Roth, M. E. Nasir, P. Segovia, A. V. Krasavin, J. Levitt, L. M. Hirvonen, B. Wells, K. Suhling, D. Richards, *et al.*, "Spontaneous emission in non-local materials," *Light: Sci. Appl.*, vol. 6, no. 6, p. e16273, 2017.

[52] Q.-Q. Wang, J.-B. Han, D.-L. Guo, S. Xiao, Y.-B. Han, H.-M. Gong, and X.-W. Zou, "Highly efficient avalanche multiphoton luminescence from coupled au nanowires in the visible region," *Nano Lett.*, vol. 7, no. 3, pp. 723–728, 2007.